Exact $(d) \mapsto (+) \& (-)$ boundary flow in the tricritical Ising model

Giovanni Feverati¹

International School for Advanced Studies, Trieste, Italy

Abstract

The integrable perturbation of the degenerate boundary condition (d) by the $\varphi_{1,3}$ boundary field generates a renormalization group flow down to the superposition of Cardy boundary states (+)&(-). Exact Thermodynamic Bethe Ansatz (TBA) equations for all the excited states are derived here extending the results of [1] to this case. As an intermediate step, the non-Cardy boundary conformal sector (+)&(-) is also described as the scaling limit of an A_4 lattice model with appropriate integrable boundary conditions and produces the first example of superposition of finitized Virasoro characters.

1 Introduction

Two dimensional quantum field theories in presence of a boundary have received an increasing attention in the last few years because of their important role in condensed matter physics (especially on quantum impurity problems) and in string theory (D-branes). Their integrable or conformal properties lead to the computation of a number of exact results (boundary S-matrices [2], conformal boundary states [3], etc. See also [4] and references indicated there). An interesting problem is to connect different boundary conformal field theories (BCFT) by integrable renormalization group flows generated by boundary operators.

The tricritical Ising model is the conformal unitary minimal model with central charge c = 7/10. Its phase diagram in presence of boundaries, with the bulk of the system maintained at the critical point, contains various fixed points (that are precisely boundary conformal field theories) connected by renormalization group flows [5, 6]. Among them, those generated by perturbing a fixed point with the magnetic boundary field $\varphi_{1,3}$ are integrable. One of the two flows departing from the BCFT (d) moves to a superposition of Cardy-type boundary states, (+)&(-). This is the simplest occurrence of the general observation [7] that the boundary interactions do not make a distinction between pure states or superposition of states. Actually, increasing the central charge of the minimal models, one expect more and more the appearance of superposition of states [8] so that the analysis presented here is a crucial step toward a quite general phenomenon. Physically speaking, boundary correlation functions of pure states satisfy the cluster property while this is not true for superposition of states. This is an indication of a first order phase transition occurring close to a BCFT that is not a pure state [6].

The flow $(d) = (2,2) \mapsto (+)\&(-) = (1,1) \oplus (3,1)$ is studied here using a lattice approach to formulate TBA equations, as described with great detail in [1] on which the present article is heavily built. For convenience, the same notations will be used. This flow was identified in [5] by the boundary S matrix; it preserves supersymmetry [9]; a TBA system for the ground state only was given [10] in a different channel (periodic).

The plan of the paper is as follows. In Section 2, the pattern of zeros for the boundary critical point $(1,1) \oplus (3,1)$ on a finite lattice will be described and the finitized partition function will appear as a superposition of finitized characters [11]. In Section 3, the flow will be recognized to be in the "variable r" family, and the mapping between finitized characters will be provided. In

¹feverati@sissa.it

Section 4, the specific set of TBA equations for this flow will be derived and numerically solved. In Appendix A there is a summary of properties of Gaussian polynomials. In Appendix B the expression for the energy at the BCFT $(1,1) \oplus (3,1)$ will be proved. In Appendix C the selection rules for the integration constants will be given, that also apply to all the cases discussed in [1].

2 The boundary critical point $(1,1) \oplus (3,1)$

An N faces double row transfer matrix with boundary conditions (r_i, a_i) , i = 1, 2 on the left/right boundaries is indicated by $\mathbf{D}_{r_1, a_1 \mid r_2, a_2}^N(u, \xi_1, \xi_2)$ where $0 < u < \lambda$ is the spectral parameter, $\lambda = \frac{\pi}{5}$ is the crossing parameter and ξ_i are parameters associated to the boundary weights. If ξ is chosen appropriately, the lattice boundary weight (r, a) scales to the conformal boundary condition [12, 13] also labeled by (r, a) [14]. In the rest of the paper, the only case that will be used is:

$$\mathbf{D}^{N}(u,\xi_{1}) = \mathbf{D}_{2,1|2,1}^{N}(u,\xi_{1},\frac{3}{2}\lambda). \tag{2.1}$$

The parameter ξ_2 will be kept fixed at the indicated value corresponding to the conformal boundary condition (2,1).

From [13], it is known that the continuum scaling limit of the double row transfer matrix $\mathbf{D}^N(\frac{\lambda}{2}, \frac{3}{2}\lambda)$ is a realization of the $(2,1)\otimes(2,1)=(1,1)\oplus(3,1)$ conformal boundary conditions. This is obtained if the boundary parameter is chosen inside the real interval $\xi_1 \in [\lambda/2, 5\lambda/2]$. The choice of the middle point of the interval will be useful later when moving off criticality by the introduction of an imaginary part for ξ_1 . The number of faces N is required to be even by the adjacency conditions.

The pattern of the zeros of the eigenvalues D(u) of $\mathbf{D}(u)$ is relevant to the classification of the states, both for the lattice and for the continuum theory, and must be determined with numerical observations performed on lattices of small size¹ N = 12 (in [1] the name "numerics on D" was used). As typical for the A_4 lattice model [12, 15], there are two analyticity strips

strip 1:
$$-\frac{\lambda}{2} < \operatorname{Re}(u) < \frac{3\lambda}{2}$$
, strip 2: $2\lambda < \operatorname{Re}(u) < 4\lambda$

and two types of strings. The 1-strings are single zeros appearing in the center of each strip

$$\operatorname{Re}(u) = \frac{\lambda}{2} \text{ or } 3\lambda$$

while the 2-strings are pairs of zeros (u, u') appearing on the edges of a strip, with the same imaginary part

$$(\operatorname{Re}(u), \operatorname{Re}(u')) = \begin{cases} (-\lambda/2, 3\lambda/2), & \text{strip } 1, \\ (2\lambda, 4\lambda), & \text{strip } 2. \end{cases}$$

In the upper half plane, let m_1 , m_2 be the number of 1-strings and n_1 , n_2 the number of 2-strings in each strip. The following relations hold between the numbers of zeros:

$$\begin{cases}
 n_1 &= \frac{N+m_2}{2} - m_1 \geqslant 0 \\
 n_2 &= \frac{m_1}{2} - m_2 + 1 \geqslant 0
 \end{cases} \Rightarrow m_1, m_2 \text{ even.}$$
(2.2)

The states on the lattice and at the scaling limit are uniquely characterized by the non-negative quantum numbers $\{I_k^{(j)}\}$; they have the topological meaning that for a given 1-string, $I_k^{(j)}$ is the number of 2-strings with larger coordinate. This remains true at the scaling limit.

¹The number of faces is mainly limited by the huge amount of RAM required to write the transfer matrix.

The determination of the scaling energy corresponding to each eigenvalue is the crucial element to distinguish states in the (1,1) or (3,1) sectors. Remembering that $\Delta_{1,1}=0$, $\Delta_{3,1}=\frac{3}{2}$, the separation between levels is quite sharp. In spite of this, the finite size effects for N=12 faces are still dominant on the accuracy of the energies, apart for the first few levels $E \leq 5$, so the complete distinction of states among the two sectors requires informations from the TBA equations that will be introduced later. Anticipating here these results, one has:

$$(1,1): I_1^{(2)} < n_2 or m_2 = 0,$$
 (2.3)

$$(3,1): I_1^{(2)} = n_2. (2.4)$$

This means that the discrimination is given by the lower object in the second strip: if it is a 2-string, the sector (1,1) is selected, if it is a 1-string the sector (3,1) is selected. The given conditions imply two useful necessary conditions for a state to be in the corresponding sector:

$$(1,1) 0 \leqslant I_1^{(2)} < n_2 \Rightarrow \frac{m_1}{2} - m_2 \geqslant 0, (2.5)$$

$$(3,1) m_2 \geqslant 2 \Rightarrow m_1 \geqslant 2. (2.6)$$

The former is an enforcement of the second expression in (2.2). The energy corresponding to each state is finally given by

$$E = -\frac{c}{24} + \frac{\mathbf{m}^{T}C\mathbf{m}}{4} - \frac{1}{2}\delta_{I_{1}^{(2)},n_{2}} + \sum_{i=1,2} \sum_{k=1}^{m_{i}} I_{k}^{(i)},$$

$$C = \begin{pmatrix} 2 & -1 \\ -1 & 2 \end{pmatrix}, \quad \delta_{a,b} : \text{ Kronecker's delta}, \quad \mathbf{m} = \begin{pmatrix} m_{1} \\ m_{2} \end{pmatrix}.$$
(2.7)

C is precisely the A_2 Cartan matrix. The complete and independent proof of this expression will be given in Appendix B.

Here a crucial observation can be done that there is a violation of the topological rule for the energy. Indeed, when only one sector is involved, if the relative position of a 1-string and a neighboring underlying 2-string are exchanged the energy increases of 1 unit. The opposite exchange reduces the energy of 1 unit [12]. Presently two sectors are considered and this rule is violated in precisely one case: if the lower objects in the second strip are a 1-string and an underlying 2-string (i.e. $I_1^{(2)} = n_2 - 1$), their exchange increases the energy of $\frac{1}{2}$ units. The opposite exchange reduces the energy of $\frac{1}{2}$ units. This corresponds to the Kronecker's delta term in (2.7). In all the other cases the usual rule holds. Notice that this violation is expected from counting arguments, namely with the usual rule only, there is no way to match the states given by $\mathbf{D}(u)$ with the states contained in $(1,1) \oplus (3,1)$. In Table 1 there is the first appearance of this violation, namely the infrared state² (0000|00), whose energy is 6, has two excitations, (0000|10), with energy $\frac{3}{2} + 5$, and (1000|00), with energy 7.

The finitized partition function is defined as a sum on the states of a finite lattice where the energy of each state is fictitiously assumed to be equal to its scaling limit energy:

$$Z_N(q) = q^{-\frac{c}{24}} \sum_{\text{states}} q^E = q^{-\frac{c}{24}} \sum_{m_1, m_2, \{I_k^{(i)}\}} q^{\frac{1}{4} \boldsymbol{m}^T C \boldsymbol{m} - \frac{1}{2} \delta_{I_1^{(2)}, n_2} + \sum_{i, k} I_k^{(i)}}$$
(2.8)

where $q = \exp(-2\pi M/N)$ is the modular parameter. Now, it will be shown that the finitized partition function matches the sum of characters. The sum on states (2.8) can be split in two

²The notation indicates the content of zeros: for example, $(3\,2\,2\,0|1\,0)$ is a state with 4 zeros in the first strip and 2 in the second; their quantum numbers are respectively $I_1^{m_1}=3$, $I_2^{m_1}=2,\ldots$ If a frozen zero occurs [12], a parity $\sigma=\pm 1$ is added.

parts, for $I_1^{(2)} < n_2$ (sector (1,1)) and for $I_1^{(2)} = n_2$ (sector (3,1)). Using the Gaussian polynomials and their properties as in Appendix A leads to:

if
$$I_1^{(2)} < n_2$$
:
$$\sum_{0 \le I_{m_2}^{(2)} \le \dots \le I_1^{(2)} < n_2} q^{I_1^{(2)} + \dots I_{m_2}^{(2)}} = \begin{bmatrix} m_2 + n_2 - 1 \\ m_2 \end{bmatrix}, \tag{2.9}$$

if
$$I_1^{(2)} = n_2$$
:
$$\sum_{0 \leqslant I_{m_2}^{(2)} \leqslant \dots \leqslant I_1^{(2)} = n_2} q^{I_1^{(2)} + \dots I_{m_2}^{(2)}} = q^{n_2} \begin{bmatrix} m_2 + n_2 - 1 \\ m_2 - 1 \end{bmatrix}.$$
 (2.10)

The sum on the first strip is not modified by this counting. The partition function now reads

$$Z_{N}(q) = q^{-\frac{c}{24}} \sum_{(1,1)} q^{\frac{1}{4}} m^{T} C m \begin{bmatrix} m_{1} + n_{1} \\ m_{1} \end{bmatrix} \begin{bmatrix} m_{2} + n_{2} - 1 \\ m_{2} \end{bmatrix}$$

$$+ q^{-\frac{c}{24}} \sum_{(3,1)} q^{\frac{1}{4}} m^{T} C m^{-\frac{1}{2}} q^{n_{2}} \begin{bmatrix} m_{1} + n_{1} \\ m_{1} \end{bmatrix} \begin{bmatrix} m_{2} + n_{2} - 1 \\ m_{2} - 1 \end{bmatrix}$$

$$(2.11)$$

where the labels on the sums indicate that the sums on m_1, m_2 are restricted by the constraints imposed by the corresponding sector (2.2-2.6). The first sum is easily recognized to be the finitized character $\chi_{1,1}^{(N)}(q)$. In the second term, the redefinition of $m_2 \to m'_2 = m_2 - 1 \ge 1$ and odd, leads to

$$\frac{1}{4}(m_1 \ m_2) C \binom{m_1}{m_2} + n_2 - \frac{1}{2} = \frac{1}{4}(m_1 \ m_2') C \binom{m_1}{m_2'}$$

so that it becomes the finitized character $\chi_{3,1}^{(N)}(q)$. This proves that the finitized partition function is the sum of the corresponding finitized characters:

$$Z_N(q) = \chi_{1,1}^{(N)}(q) + \chi_{3,1}^{(N)}(q)$$
(2.12)

and, consequently, that the pattern of zeros (2.2) and the distinction of sectors (2.3, 2.4) are consistent with the known scaling properties of the given transfer matrix.

3 The flow: 3 mechanisms

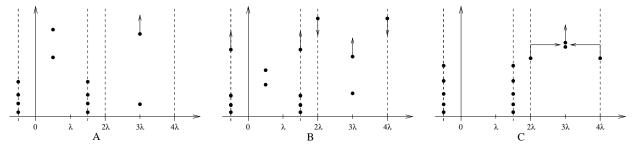


Fig. 1. The three mechanisms A, B, C respectively that change string content during the flow $\chi_{1,1} + \chi_{3,1} \mapsto \chi_{2,2}$ which is the reverse of the physical flow. These mechanisms are illustrated for the states: A, $(0\,0|0\,0) \mapsto (0\,0|0)_+$; B, $(1\,1|0\,0) \mapsto (0\,0|1)_-$; C, $() \mapsto (|0)_-$.

Considering the transfer matrix $\mathbf{D}(u, \xi_{\text{latt}})$ with $\xi_{\text{latt}} = \frac{3}{2}\lambda + i\xi/5$, one can compute the expected endpoints,

$$\mathbf{D}^{N}(u, \frac{3}{2}\lambda + i\frac{\xi}{5}) \longrightarrow \begin{cases} \chi_{2,2} & \text{if } \xi \to \pm \infty \\ \chi_{1,1} + \chi_{3,1} & \text{if } \xi = 0 \end{cases}$$
 (3.1)

Table 1. Flow $\chi_{1,1} + \chi_{3,1} \mapsto \chi_{2,2}$ (reverse of the physical flow). The explicit mapping of states from IR to UV up to the IR level 7 are presented here. $n^{\rm IR}$, $n^{\rm UV}$ are the excitation levels above the ground states, respectively $\Delta_{1,1} = 0$ and $\Delta_{2,2} = \frac{3}{80}$. The IR states in the two sectors are easily recognized because in (3,1) they are separated by $\Delta_{3,1} = \frac{3}{2}$ from the true ground state.

n^{IR}	mapping of states, mechanism			n^{UV}	n^{IR}	mapping of states, mechanism		n^{UV}	
0	()	$\overset{\mathrm{C}}{\mapsto}$	$(0)_{-}$	0	$\frac{3}{2} + 4$	(31 00)	$\overset{\mathrm{B}}{\mapsto}$	$(20 1)_{-}$	5
$\frac{3}{2}$	(00 00)	$\overset{A}{\mapsto}$	$(00 0)_{+}$	1	$\frac{3}{2} + 4$	(22 00)	$\overset{\mathrm{B}}{\mapsto}$	$(11 1)_{-}$	5
2	(00)	$\overset{\mathrm{C}}{\mapsto}$	$(00 0)_{-}$	2	6	(0000 00)	$\overset{A}{\mapsto}$	$(0000 0)_{+}$	5
$\frac{3}{2} + 1$	(10 00)	$\overset{A}{\mapsto}$	$(10 0)_{+}$	2	6	(40)	$\overset{\mathrm{C}}{\mapsto}$	$(40 0)_{-}$	6
3	(10)	$\overset{\mathrm{C}}{\mapsto}$	$(10 0)_{-}$	3	6	(31)	$\overset{\mathrm{C}}{\mapsto}$	$(31 0)_{-}$	6
$\frac{3}{2} + 2$	(20 00)	$\overset{A}{\mapsto}$	$(20 0)_{+}$	3	6	(22)	$\overset{\mathrm{C}}{\mapsto}$	$(22 0)_{-}$	6
$\frac{3}{2} + 2$	(11 00)	$\stackrel{\mathrm{B}}{\mapsto}$	$(00 1)_{-}$	3	$\frac{3}{2} + 5$	(0000 10)	$\overset{A}{\mapsto}$	$(0000 1)_{+}$	6
4	(20)	$\overset{\mathrm{C}}{\mapsto}$	$(20 0)_{-}$	4	$\frac{3}{2} + 5$	(50 00)	$\overset{A}{\mapsto}$	$(50 0)_{+}$	6
4	(11)	$\overset{\mathrm{C}}{\mapsto}$	$(11 0)_{-}$	4	$\frac{3}{2} + 5$	(41 00)	$\overset{\mathrm{B}}{\mapsto}$	$(30 1)_{-}$	6
$\frac{3}{2} + 3$	(30 00)	$\overset{A}{\mapsto}$	$(30 0)_{+}$	4	$\frac{3}{2} + 5$	(32 00)	$\overset{\mathrm{B}}{\mapsto}$	$(21 1)_{-}$	6
$\frac{3}{2} + 3$	(21 00)	$\overset{\mathrm{B}}{\mapsto}$	$(10 1)_{-}$	4	7	(1000 00)	$\overset{A}{\mapsto}$	$(1000 0)_{+}$	6
5	(30)	$\overset{C}{\mapsto}$	$(30 0)_{-}$	5	7	(50)	$\overset{\mathrm{C}}{\mapsto}$	$(50 0)_{-}$	7
5	(21)	$\overset{C}{\mapsto}$	$(21 0)_{-}$	5	7	(41)	$\overset{C}{\mapsto}$	$(41 0)_{-}$	7
$\frac{3}{2} + 4$	(40 00)	$\overset{A}{\mapsto}$	$(40 0)_{+}$	5	7	(32)	$\overset{\mathrm{C}}{\mapsto}$	$(32 0)_{-}$	7

as it was done in [1] for various types of boundary. The choice of the real part $\text{Re}(\xi_{\text{latt}}) = \frac{3}{2}\lambda$ makes the double row transfer matrix real symmetric on the center of each strip, $\text{Re}(u) = \frac{\lambda}{2}$, 3λ so that the eigenvalues and the energies are real. Any different value for the real part would lead to complex energies and non-unitary flows. Summarizing, one has integrability, correct endpoints, unitarity, and uniqueness so the identification of this lattice flow with the renormalization flow $(2,2) \to (1,1) \oplus (3,1)$ is completely natural.

From extensive "numerics on D" one can figure out the correspondence between infrared (IR) and ultraviolet (UV) states, Table 1, and the three mechanisms A, B, C active to change the pattern of zeros. They are the same known for the "variable r" flows in [1] so the present flow is part of that family. For their complete description the reader is referred to [1] while here there is a summary of the properties and in Fig. 1 there is an example of their action.

The mechanisms A,B,C force the following changes for the various parameters:

A.
$$I_{m_1}^{(1)} = I_{m_2^{\text{IR}}}^{(2)}^{\text{IR}} = 0$$
:
 $m_2^{\text{IR}} \mapsto m_2^{\text{UV}} = m_2^{\text{IR}} - 1, \qquad \sigma = 1.$ (3.2)

B.
$$I_{m_1}^{(1)^{\mathrm{IR}}} > 0$$
, $I_{m_2^{\mathrm{IR}}}^{(2)^{\mathrm{IR}}} = 0$:
$$m_2^{\mathrm{IR}} \mapsto m_2^{\mathrm{UV}} = m_2^{\mathrm{IR}} - 1, \qquad \sigma = -1,$$

$$I_k^{(1)^{\mathrm{IR}}} \mapsto I_k^{(1)^{\mathrm{UV}}} = I_k^{(1)^{\mathrm{IR}}} - 1, \qquad k = 1, \dots, m_1,$$

$$I_k^{(2)^{\mathrm{IR}}} \mapsto I_k^{(2)^{\mathrm{UV}}} = I_k^{(2)^{\mathrm{IR}}} + 1, \qquad k = 1, \dots, m_2^{\mathrm{IR}} - 1,$$

$$n_1^{\mathrm{IR}} \mapsto n_1^{\mathrm{UV}} = n_1^{\mathrm{IR}} - 1,$$

$$n_2^{\mathrm{IR}} \mapsto n_2^{\mathrm{UV}} = n_2^{\mathrm{IR}} + 1.$$

$$(3.3)$$

C.
$$I_{m_2^{\text{IR}}}^{(2)} > 0$$
:

$$m_2^{\text{IR}} \mapsto m_2^{\text{UV}} = m_2^{\text{IR}} + 1, \qquad \sigma = -1, \qquad I_{m_2^{\text{UV}}}^{(2)} = 0,$$

$$I_k^{(2)^{\text{IR}}} \mapsto I_k^{(2)^{\text{UV}}} = I_k^{(2)^{\text{IR}}} - 1, \qquad k = 1, \dots, m_2^{\text{IR}},$$

$$n_2^{\text{IR}} \mapsto n_2^{\text{UV}} = n_2^{\text{IR}} - 1.$$
(3.4)

where no label IR or UV is used for parameters that do not change during the flow.

An important consistency check is to show that the three mechanisms respect the counting of states at the endpoints of the flow. From (3.2, 3.3, 3.4) one sees that for each IR state there is precisely one applicable mechanism so that the IR counting of states is complete. Moreover, using the recoursive identities among Gaussian polynomials (A.2, A.3) the IR partition function in (2.11) naturally splits into six terms precisely associated with the three mechanisms, one for each sector:

$$q^{\frac{c}{24}}Z_{N}^{IR}(q) = \sum_{(1,1)A} q^{\frac{1}{4}\boldsymbol{m}^{IR}}C\boldsymbol{m}^{IR} \begin{bmatrix} m_{1} + n_{1}^{IR} - 1 \\ m_{1} - 1 \end{bmatrix} \begin{bmatrix} m_{2}^{IR} + n_{2}^{IR} - 2 \\ m_{2}^{IR} - 1 \end{bmatrix}$$

$$+ \sum_{(1,1)B} q^{\frac{1}{4}\boldsymbol{m}^{IR}}C\boldsymbol{m}^{IR} q^{m_{1}} \begin{bmatrix} m_{1} + n_{1}^{IR} - 1 \\ m_{1} \end{bmatrix} \begin{bmatrix} m_{2}^{IR} + n_{2}^{IR} - 2 \\ m_{2}^{IR} - 1 \end{bmatrix}$$

$$+ \sum_{(1,1)C} q^{\frac{1}{4}\boldsymbol{m}^{IR}}C\boldsymbol{m}^{IR} q^{m_{2}^{IR}} \begin{bmatrix} m_{1} + n_{1}^{IR} \\ m_{1} \end{bmatrix} \begin{bmatrix} m_{2}^{IR} + n_{2}^{IR} - 2 \\ m_{2}^{IR} \end{bmatrix}$$

$$+ \sum_{(3,1)A} q^{\frac{1}{4}\boldsymbol{m}^{IR}}C\boldsymbol{m}^{IR} - \frac{1}{2}q^{n_{2}^{IR}} \begin{bmatrix} m_{1} + n_{1}^{IR} - 1 \\ m_{1} - 1 \end{bmatrix} \begin{bmatrix} m_{2}^{IR} + n_{2}^{IR} - 2 \\ m_{2}^{IR} - 2 \end{bmatrix}$$

$$+ \sum_{(3,1)B} q^{\frac{1}{4}\boldsymbol{m}^{IR}}C\boldsymbol{m}^{IR} - \frac{1}{2}q^{n_{2}^{IR}} + m_{1}^{IR} \begin{bmatrix} m_{1} + n_{1}^{IR} - 1 \\ m_{1} \end{bmatrix} \begin{bmatrix} m_{2}^{IR} + n_{2}^{IR} - 2 \\ m_{2}^{IR} - 2 \end{bmatrix}$$

$$+ \sum_{(3,1)C} q^{\frac{1}{4}\boldsymbol{m}^{IR}}C\boldsymbol{m}^{IR} - \frac{1}{2}q^{n_{2}^{IR}} + m_{2}^{IR} \begin{bmatrix} m_{1} + n_{1}^{IR} \\ m_{1} \end{bmatrix} \begin{bmatrix} m_{2}^{IR} + n_{2}^{IR} - 2 \\ m_{2}^{IR} - 1 \end{bmatrix} .$$

$$+ \sum_{(3,1)C} q^{\frac{1}{4}\boldsymbol{m}^{IR}}C\boldsymbol{m}^{IR} - \frac{1}{2}q^{n_{2}^{IR}} + m_{2}^{IR} \begin{bmatrix} m_{1} + n_{1}^{IR} \\ m_{1} \end{bmatrix} \begin{bmatrix} m_{2}^{IR} + n_{2}^{IR} - 2 \\ m_{2}^{IR} - 1 \end{bmatrix} .$$

The labels (1,1), (3,1), A, B, C indicate that the corresponding sums on m_1 , $m_2^{\rm IR}$ are restricted by the constraints imposed by the respective sector and mechanism. Notice that in the (1,1) sector the quantum numbers in the second strip are bounded by $I_1^{(2)} = n_2^{\rm IR} = 1$ while in the sector (3,1) the value $I_1^{(2)} = n_2^{\rm IR}$ is fixed and doesn't enter the combinatorics that is equivalent to say that

 $m_2^{\text{IR}} - 1$ zeros must be considered. The two sum constrained by A can be understood using (A.5) for both the q-binomial factors and correspond to summing under the constraint $I_{m_1}^{(1)} = I_{m_2^{\text{IR}}}^{(2)} = 0$.

Similarly, the sum on B becomes apparent using (A.4) for the first strip q-binomial and (A.5) for the second strip q-binomial and likewise the sum on C uses (A.4) for the second strip only.

Two steps are now involved: the first is the mapping of energies, the second is the counting of states. The IR energy expression is given by (2.7). For the UV sector (2,2) is given here [12]:

$$E = -\frac{c}{24} + \Delta_{2,2} + \frac{\mathbf{m}^T C \mathbf{m}}{4} - \frac{\sigma}{2} (m_1 - m_2) + \sum_{i=1,2} \sum_{k=1}^{m_i} I_k^{(i)},$$
(3.6)

 $\Delta_{2,2} = \frac{3}{80}$; the rules for the various parameters are given in Table 2. An IR energy level at the base of a tower of states with string content fixed by $(m_1, m_2^{\rm IR})$ maps to a UV energy level according to the energy expressions (2.7, 3.6) that hold at the two conformal endpoints of the flow

$$(1,1) \begin{cases} A: & q^{\frac{1}{4}\boldsymbol{m}^{\mathrm{IR}}C\boldsymbol{m}^{\mathrm{IR}}} & \mapsto q^{\Delta_{2,2}} q^{\frac{1}{4}\boldsymbol{m}^{\mathrm{UV}}C\boldsymbol{m}^{\mathrm{UV}}} q^{-\frac{1}{2}(m_{1}-m_{2}^{\mathrm{UV}})} \\ B: & q^{\frac{1}{4}\boldsymbol{m}^{\mathrm{IR}}C\boldsymbol{m}^{\mathrm{IR}}} q^{m_{1}} & \mapsto q^{\Delta_{2,2}} q^{\frac{1}{4}\boldsymbol{m}^{\mathrm{UV}}C\boldsymbol{m}^{\mathrm{UV}}} q^{m_{2}^{\mathrm{UV}}} q^{+\frac{1}{2}(m_{1}-m_{2}^{\mathrm{UV}})} \\ C: & q^{\frac{1}{4}\boldsymbol{m}^{\mathrm{IR}}C\boldsymbol{m}^{\mathrm{IR}}} q^{m_{2}^{\mathrm{IR}}} & \mapsto q^{\Delta_{2,2}} q^{\frac{1}{4}\boldsymbol{m}^{\mathrm{UV}}C\boldsymbol{m}^{\mathrm{UV}}} q^{+\frac{1}{2}(m_{1}-m_{2}^{\mathrm{UV}})} \\ A: & q^{\frac{1}{4}\boldsymbol{m}^{\mathrm{IR}}C\boldsymbol{m}^{\mathrm{IR}}-\frac{1}{2}+n_{2}^{\mathrm{IR}}} & \mapsto q^{\Delta_{2,2}} q^{\frac{1}{4}\boldsymbol{m}^{\mathrm{UV}}C\boldsymbol{m}^{\mathrm{UV}}+n_{2}^{\mathrm{UV}}} q^{-\frac{1}{2}(m_{1}-m_{2}^{\mathrm{UV}})} \\ B: & q^{\frac{1}{4}\boldsymbol{m}^{\mathrm{IR}}C\boldsymbol{m}^{\mathrm{IR}}-\frac{1}{2}+n_{2}^{\mathrm{IR}}} q^{m_{1}} & \mapsto q^{\Delta_{2,2}} q^{\frac{1}{4}\boldsymbol{m}^{\mathrm{UV}}C\boldsymbol{m}^{\mathrm{UV}}+n_{2}^{\mathrm{UV}}-1} q^{m_{2}^{\mathrm{UV}}} q^{+\frac{1}{2}(m_{1}-m_{2}^{\mathrm{UV}})} \\ C: & q^{\frac{1}{4}\boldsymbol{m}^{\mathrm{IR}}C\boldsymbol{m}^{\mathrm{IR}}-\frac{1}{2}+n_{2}^{\mathrm{IR}}} q^{m_{2}^{\mathrm{IR}}} & \mapsto q^{\Delta_{2,2}} q^{\frac{1}{4}\boldsymbol{m}^{\mathrm{UV}}C\boldsymbol{m}^{\mathrm{UV}}+n_{2}^{\mathrm{UV}}} q^{+\frac{1}{2}(m_{1}-m_{2}^{\mathrm{UV}})}. \end{cases} \end{cases}$$

Using (3.2) to (3.4), the q-binomials appearing in the IR partition function (3.5) are rewritten in terms of UV parameters. Also taking into account the mapping of the energies (3.7) one obtains:

$$q^{\frac{c}{24}}Z_{N}^{IR}(q) \mapsto q^{\Delta_{2,2}} \left\{ \sum_{(1,1)A} q^{\frac{1}{4}\boldsymbol{m}^{\mathrm{UV}}C\boldsymbol{m}^{\mathrm{UV}}} q^{-\frac{1}{2}(m_{1}-m_{2}^{\mathrm{UV}})} \begin{bmatrix} m_{1}+n_{1}^{\mathrm{UV}}-1 \\ m_{1}-1 \end{bmatrix} \begin{bmatrix} m_{2}^{\mathrm{UV}}+n_{2}^{\mathrm{UV}}-1 \\ m_{2}^{\mathrm{UV}} \end{bmatrix} \right. \\ + \sum_{(1,1)B} q^{\frac{1}{4}\boldsymbol{m}^{\mathrm{UV}}C\boldsymbol{m}^{\mathrm{UV}}} q^{\frac{1}{2}(m_{1}-m_{2}^{\mathrm{UV}})} q^{m_{2}^{\mathrm{UV}}} \begin{bmatrix} m_{1}+n_{1}^{\mathrm{UV}} \\ m_{1} \end{bmatrix} \begin{bmatrix} m_{2}^{\mathrm{UV}}+n_{2}^{\mathrm{UV}}-2 \\ m_{2}^{\mathrm{UV}} \end{bmatrix} \\ + \sum_{(1,1)C} q^{\frac{1}{4}\boldsymbol{m}^{\mathrm{UV}}C\boldsymbol{m}^{\mathrm{UV}}} q^{\frac{1}{2}(m_{1}-m_{2}^{\mathrm{UV}})} \begin{bmatrix} m_{1}+n_{1}^{\mathrm{UV}} \\ m_{1} \end{bmatrix} \begin{bmatrix} m_{2}^{\mathrm{UV}}+n_{2}^{\mathrm{UV}}-2 \\ m_{2}^{\mathrm{UV}}-1 \end{bmatrix} \\ + \sum_{(3,1)A} q^{\frac{1}{4}\boldsymbol{m}^{\mathrm{UV}}C\boldsymbol{m}^{\mathrm{UV}}} q^{-\frac{1}{2}(m_{1}-m_{2}^{\mathrm{UV}})} \begin{bmatrix} m_{1}+n_{1}^{\mathrm{UV}}-1 \\ m_{1}-1 \end{bmatrix} \begin{bmatrix} m_{2}^{\mathrm{UV}}+n_{2}^{\mathrm{UV}}-1 \\ m_{2}^{\mathrm{UV}}-1 \end{bmatrix} \\ + \sum_{(3,1)B} q^{\frac{1}{4}\boldsymbol{m}^{\mathrm{UV}}C\boldsymbol{m}^{\mathrm{UV}}} q^{\frac{1}{2}(m_{1}-m_{2}^{\mathrm{UV}})} q^{n_{2}^{\mathrm{UV}}-1+m_{2}^{\mathrm{UV}}} \begin{bmatrix} m_{1}+n_{1}^{\mathrm{UV}} \\ m_{1} \end{bmatrix} \begin{bmatrix} m_{2}^{\mathrm{UV}}+n_{2}^{\mathrm{UV}}-2 \\ m_{2}^{\mathrm{UV}}-1 \end{bmatrix} \\ + \sum_{(3,1)C} q^{\frac{1}{4}\boldsymbol{m}^{\mathrm{UV}}C\boldsymbol{m}^{\mathrm{UV}}} q^{\frac{1}{2}(m_{1}-m_{2}^{\mathrm{UV}})+n_{2}^{\mathrm{UV}}} \begin{bmatrix} m_{1}+n_{1}^{\mathrm{UV}} \\ m_{1} \end{bmatrix} \begin{bmatrix} m_{2}^{\mathrm{UV}}+n_{2}^{\mathrm{UV}}-2 \\ m_{2}^{\mathrm{UV}}-2 \end{bmatrix} \right\}.$$

The two terms corresponding to each mechanism can be summed with (A.3) so that the distinction

among sectors disappear

$$q^{\frac{c}{24}}Z_{N}^{IR}(q) \mapsto q^{\Delta_{2,2}} \left\{ \sum_{A} q^{\frac{1}{4}\boldsymbol{m}^{\mathrm{UV}}C\boldsymbol{m}^{\mathrm{UV}}} q^{-\frac{1}{2}(m_{1}-m_{2}^{\mathrm{UV}})} \begin{bmatrix} m_{1}+n_{1}^{\mathrm{UV}}-1 \\ m_{1}-1 \end{bmatrix} \begin{bmatrix} m_{2}^{\mathrm{UV}}+n_{2}^{\mathrm{UV}} \\ m_{2}^{\mathrm{UV}} \end{bmatrix} \right. \\ + \sum_{B} q^{\frac{1}{4}\boldsymbol{m}^{\mathrm{UV}}C\boldsymbol{m}^{\mathrm{UV}}} q^{\frac{1}{2}(m_{1}-m_{2}^{\mathrm{UV}})} q^{m_{2}^{\mathrm{UV}}} \begin{bmatrix} m_{1}+n_{1}^{\mathrm{UV}} \\ m_{1} \end{bmatrix} \begin{bmatrix} m_{2}^{\mathrm{UV}}+n_{2}^{\mathrm{UV}}-1 \\ m_{2}^{\mathrm{UV}} \end{bmatrix} \\ + \sum_{C} q^{\frac{1}{4}\boldsymbol{m}^{\mathrm{UV}}C\boldsymbol{m}^{\mathrm{UV}}} q^{\frac{1}{2}(m_{1}-m_{2}^{\mathrm{UV}})} \begin{bmatrix} m_{1}+n_{1}^{\mathrm{UV}} \\ m_{1} \end{bmatrix} \begin{bmatrix} m_{2}^{\mathrm{UV}}+n_{2}^{\mathrm{UV}}-1 \\ m_{2}^{\mathrm{UV}}-1 \end{bmatrix} \right\} \\ = q^{\Delta_{2,2}} \sum_{\sigma=\pm 1} \sum_{m_{1},m_{2}^{\mathrm{UV}}} q^{\frac{1}{4}\boldsymbol{m}^{\mathrm{UV}}C\boldsymbol{m}^{\mathrm{UV}}} q^{-\frac{\sigma}{2}(m_{1}-m_{2}^{\mathrm{UV}})} \begin{bmatrix} m_{1}+n_{1}^{\mathrm{UV}}-\delta_{\sigma,1} \\ m_{1}-\delta_{\sigma,1} \end{bmatrix} \begin{bmatrix} m_{2}^{\mathrm{UV}}+n_{2}^{\mathrm{UV}} \\ m_{2}^{\mathrm{UV}} \end{bmatrix} \\ = q^{\frac{c}{24}} \chi_{2,2}^{(N)}(q)$$

$$(3.9)$$

and one is left with the UV partition function, that is the (2, 2) finitized character. This argument shows that the IR counting of states with the three mechanisms induces the correct UV counting of states.

4 The flow: TBA equations

The TBA equations are obtained with the procedure given in [1]: the double row transfer matrix (2.1) eigenvalues can be normalized such that they satisfy a functional equation. The analytic content of the normalized transfer matrix eigenvalues is used to solve by Fourier transform the functional equation. As last step, a scaling limit is performed to obtain the equations for a continuum theory (TBA equations). The normalization factor is highly non-trivial in the sense that it contains both the spectral and the boundary parameter. The latter appears by a factor $g(u, \xi_{\text{latt}})$ that is common to all the "variable r" cases and, with reference to the center lines of the two analyticity strips and at the scaling limit, is given by:

$$\hat{g}_1(x,\xi) = \tanh \frac{x+\xi}{2},\tag{4.1}$$

$$\hat{g}_2(x,\xi) = 1.$$
 (4.2)

This procedure leads to the same TBA equations, energy expression and quantization conditions known [1] for the "variable r" flows:

$$\epsilon_1(x) = -\log \hat{g}_1(x,\xi) - \sum_{k=1}^{m_1} \log(\tanh \frac{y_k^{(1)} - x}{2}) - K * L_2,$$
(4.3)

$$\epsilon_2(x) = 4e^{-x} - \log \hat{g}_2(x,\xi) - \sum_{k=1}^{m_2} \log(\tanh \frac{y_k^{(2)} - x}{2}) - K * L_1$$
(4.4)

where the integration kernel is given by $K(x) = \frac{1}{2\pi \cosh x}$ and $L_j(x) = \log |1 + s_j \exp(-\epsilon_j)|$. The *denotes the convolution, $(f * g)(x) = \int_{-\infty}^{+\infty} dy \, f(x - y)g(y)$. The energy expression is

$$E(\xi) = \frac{2}{\pi} \sum_{k=1}^{m_1} e^{-y_k^{(1)}} - \int_{-\infty}^{\infty} \frac{dx}{\pi^2} e^{-x} L_2$$
 (4.5)

Table 2. Classification of the patterns of 1- and 2-strings at the endpoints of the flow. The parity $\sigma = \pm 1$ occurs in (2,2) because there are frozen zeros. The parities $s_1, s_2 = \pm 1$ occur in the TBA equations as integration constants (see Appendix C). The expressions for n_1 are only used on a finite lattice because in the scaling limit $n_1 \sim N/2 \to \infty$. The number of faces in a row, N, is even.

$\chi_{r,s}(q)$	$(\boldsymbol{m}, \boldsymbol{n})$ system	int. const.	quantum numbers		
$\chi_{2,2}^{(N)}(q)$	m_1 even, m_2 odd	$s_1 = -1$	$n_k^{(1)} = 2(I_k^{(1)} + m_1 - k) + 1 - m_2 - \sigma$		
$\chi_{2,2}(q)$	$n_2 = (m_1 - \sigma + 1)/2 - m_2$ $n_1 = (N + m_2 + \sigma)/2 - m_1$	$s_2 = 1$	$n_k^{(2)} = 2(I_k^{(2)} + m_2 - k) + 1 - m_1 + \sigma$		
$\chi_{1.1}^{(N)}(q)$	$(1,1): m_1, m_2 \text{ even}$	$s_2 = 1$	(1) $\Omega(I^{(1)} + I) + 1$		
$\begin{pmatrix} \chi_{1,1}(q) \\ +\chi_{3,1}^{(N)}(q) \end{pmatrix}$	$(3,1): m_1 \text{ even}, m_2 \text{ odd}$	$s_2 = -1$	$n_k^{(1)} = 2(I_k^{(1)} + m_1 - k) + 1 - m_2$		
	$n_2 = m_1/2 - m_2 + 1$	$s_1 = 1$	$n_k^{(2)} = 2(I_k^{(2)} + m_2 - k) + 1 - m_1$		
1,73,1 (4)	$n_1 = (N + m_2)/2 - m_1$				

and the quantization conditions are expressed in terms of the counting functions [1] $\psi_j(x) = -i\epsilon_j(x-i\frac{\pi}{2})$:

$$\psi_2(y_k^{(1)}) = -i\,\epsilon_2(y_k^{(1)} - i\frac{\pi}{2}) = n_k^{(1)}\pi, \qquad n_k^{(1)} = 2(I_k^{(1)} + m_1 - k) + 1 - m_2, \tag{4.6}$$

$$\psi_1(y_k^{(2)}) = -i\,\epsilon_1(y_k^{(2)} - i\frac{\pi}{2}) = n_k^{(2)}\pi, \qquad n_k^{(2)} = 2(I_k^{(2)} + m_2 - k) + 1 - m_1. \tag{4.7}$$

Note the inversion of the indices: ϵ_1 is for strip 2 and ϵ_2 for strip 1. This set of equations gives the complete description of the scaling energy for all the states of the flow under examination. The correct choice of the parameters m_i , n_2 is suggested by the lattice (Section 2) and a quick numerical check on the ground state leads to the values of the integration constants s_i . In summary, starting close to the IR point $(\xi \to +\infty)$ and moving along the flow one has:

mechanism A and B, mechanism C before the collapse:

$$m_1, m_2$$
 even, $n_2 = \frac{m_1}{2} - m_2 + 1 \ge 0, \quad s_1 = s_2 = 1,$

mechanism C after the collapse point:

$$m_2^A = m_2 + 2$$
, $n_{m_2^A - 1}^{(2)} = n_{m_2^A}^{(2)} = 1 - m_1$, the other variables remain unchanged.

A small surprise is given at the IR point itself: performing the limit $\xi \to +\infty$ on the TBA equations leads to two different setups for the two sectors, namely the previous summary is correct for both the sectors along the flow and for the sector (1,1) only at the IR point. The sector (3,1) at the IR point requires an odd number of 1-strings in strip 2 as well as $s_2 = -1$, as shown in Table 2. This odd behaviour of the flow close to the IR point is new: in all the previous cases, the movement off the IR point was observed to be smooth and the content of zeros never came up with a change in the value of m_2 . The reason can be easily found in the discontinuity of the following limit (eq. (3.70) of [1]):

$$\lim_{x \to -\infty} \psi_1(x) = \lim_{x \to -\infty} i \log \hat{g}_1(x, \xi) = \begin{cases} \pi & \text{if } \xi < +\infty, \\ 0 & \text{if } \xi = +\infty \end{cases}$$
 (4.8)

In the first case, the odd parity of $n_k^{(2)}$ (4.7) implies that a second strip zero can be found at $-\infty$. Indeed, a clear numerical evidence and the following simple argument show that $y_1^{(2)} = -\infty$ precisely for all the states in the (3,1) sector. Looking at the difference between the endpoints of

 ψ_1 along the flow (assuming $y_{m_1}^{(1)} < +\infty$) one has

$$\lim_{x \to -\infty} \psi_1(x) - \lim_{x \to +\infty} \psi_1(x) = \pi(1 + m_1) = \pi \cdot \text{``odd''}$$
 (4.9)

so that the maximum number of zeros (1- and 2-strings) that find room in that interval³ is $\lfloor \frac{m_1+1}{2} \rfloor + 1 = \frac{m_1}{2} + 1$ that coincides with the actual number of 1- and 2-strings in the strip, $m_2 + n_2$. So, all the locations are full and when $I_1^{(2)} = n_2$, equivalent to the (3,1) sector, the lowest location must be occupied by a 1-string. Observe that the alternative assumption $y_{m_1}^{(1)} = +\infty$ leads to the same conclusion because m_1 is even. Summarizing, along the flow one has $y_1^{(2)} = -\infty$; in the IR limit $\xi \to +\infty$ this zero must leave the complex plane because of the second case in (4.8) and this leads to the rules for the TBA in (3,1) sector, as in Table 2.

A numerical solution of this set of TBA equations for the first few states was done and is given in Fig. 2.

5 Conclusions

The lattice approach to boundary renormalization flows exposed in [1] and extended here appears quite effective in obtaining the scaling energy for all the excitations. It should be interesting to understand something more about the role played by the picture of zeros in the continuum theory itself. Indeed, this structure survives the scaling limit and is relevant in the description of states.

Moreover, there are structures that are common to the $\varphi_{1,3}$ perturbations [15] of tricritical Ising model. They are the types of zeros and number of strips, corresponding to the number of pseudoenergies, the way these pseudoenergies are coupled to form the TBA system and the kernel. It should be nice to have track of this from the continuum theory itself.

It is also an interesting open question to extend the present lattice approach to all the boundary flows for the whole series A-D-E of minimal models.

Acknowledgments

The author would like to thank P. Pearce and F. Ravanini for having read the manuscript. The content of Appendix C comes from a private discussion with P. Pearce.

Appendix A. Gaussian polynomials

The finitized characters are know to be expressed in terms of q-binomials. They are combinatorial expressions defined by:

$$\begin{bmatrix} m+n \\ m \end{bmatrix} = \sum_{I_1=0}^{n} \sum_{I_2=0}^{I_1} \cdots \sum_{I_m=0}^{I_{m-1}} q^{I_1+\dots+I_m}. \tag{A.1}$$

Two recoursive relations are important for this paper:

$$\begin{bmatrix} m+n \\ m \end{bmatrix} = \begin{bmatrix} m+n-1 \\ m-1 \end{bmatrix} + q^m \begin{bmatrix} m+n-1 \\ m \end{bmatrix}, \tag{A.2}$$

$$\begin{bmatrix} m+n \\ m \end{bmatrix} = \begin{bmatrix} m+n-1 \\ m \end{bmatrix} + q^n \begin{bmatrix} m+n-1 \\ m-1 \end{bmatrix}.$$
(A.3)

[[]x] means the integer part of x.

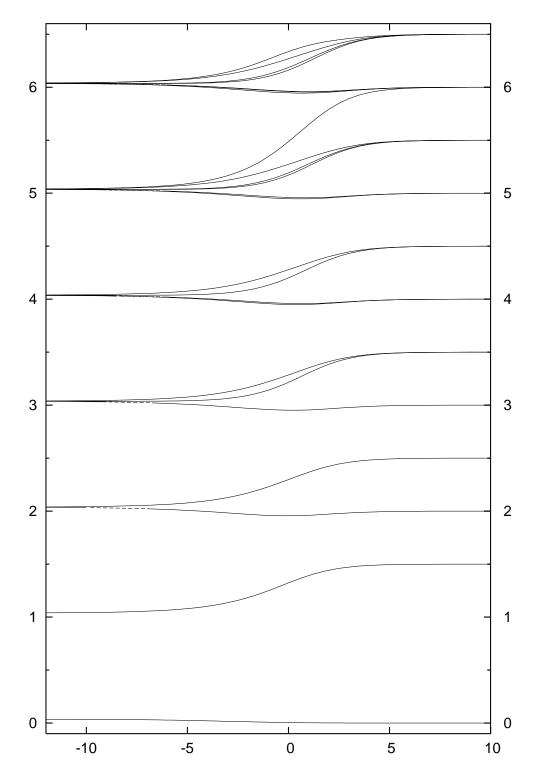


Fig. 2. Scaling energies for the flow $\chi_{2,2} \mapsto \chi_{1,1} + \chi_{3,1}$. The list of states is given in Table 1. The intermediate region of the mechanism C levels (shown dashed) are schematic and have not been obtained from the solution of the TBA equations.

The following expressions are useful to understand the contribution of each mechanism to the full character. Indeed, the restriction $I_m > 0$ leads to

$$\sum_{I_1=1}^{n} \sum_{I_2=1}^{I_1} \dots \sum_{I_m=1}^{I_{m-1}} q^{I_1+\dots+I_m} = q^m \sum_{I_1'=0}^{n-1} \sum_{I_2'=0}^{I_1'} \dots \sum_{I_m'=0}^{I_{m-1}'} q^{I_1'+\dots+I_m'} = q^m \begin{bmatrix} m+n-1 \\ m \end{bmatrix}$$
(A.4)

whereas the restriction $I_m = 0$ leads to

$$\sum_{I_1=0}^n \sum_{I_2=0}^{I_1} \dots \sum_{I_{m-1}=0}^{I_{m-2}} q^{I_1 + \dots + I_{m-1}} = \begin{bmatrix} m+n-1 \\ m-1 \end{bmatrix}.$$
 (A.5)

Appendix B. Proof of the expression for the energy at $(1,1) \oplus (3,1)$

The energy expression (2.7) is proved here using the continuum energy and the TBA equations in the limit $\xi \to +\infty$. The method is similar to the computation done in [12] at each critical point but, in the present case, one has to consider extra terms that appear because the limit $\xi \to +\infty$ will be taken only at the end of the computation.

The first step is to transform (4.5) in a more explicit form. Its first term, $e^{-y_k^{(1)}}$, can be expressed by the quantization condition (4.6) and then one adds $0 = \sum_{k=1}^{m_2} (n_k^{(2)} \pi - \psi_1(y_k^{(2)}))$ from (4.7). Some numeric terms are obtained, given by sums and products of m_i and integer numbers. They can be easily worked out with the help of the Cartan matrix defined in (2.7) leading to

$$E(\xi) = \frac{\boldsymbol{m}^{T}C\boldsymbol{m}}{4} + \sum_{i=1}^{2} \sum_{k=1}^{m_{i}} I_{k}^{(i)} - \frac{i}{2\pi} \sum_{k=1}^{m_{2}} \log \hat{g}_{1}(y_{k}^{(2)} - i\frac{\pi}{2}, \xi)$$

$$+ \int_{-\infty}^{+\infty} \frac{dx}{4\pi^{2}} \left[\sum_{k=1}^{m_{1}} \frac{L_{1}(x)}{\sinh(y_{k}^{(1)} - x)} + \sum_{k=1}^{m_{2}} \frac{L_{2}(x)}{\sinh(y_{k}^{(2)} - x)} - 4e^{-x}L_{2}(x) \right].$$
(B.1)

The contribution from the integration can be worked out with the following procedure. The main point is to compute, in two different ways, the real integral:

$$S_{j} = \int_{-\infty}^{+\infty} dx \left[-\epsilon'_{j} L_{j} + \operatorname{Re}(\epsilon_{j}) L'_{j} \right]$$

$$= \int_{-\infty}^{+\infty} dx \left[(\log s_{j} \hat{t}_{j})' \log |1 + \hat{t}_{j}| - \operatorname{Re}(\log(s_{j} \hat{t}_{j}))(\log |1 + \hat{t}_{j}|)' \right]$$
(B.2)

where $\hat{t}_j = s_j \exp(-\epsilon_j)$. On the first hand, the real axis is divided in the following intervals

$$\int_{-\infty}^{+\infty} = \int_{-\infty}^{y_1^{(j)}} + \int_{y_1^{(j)}}^{y_2^{(j)}} + \dots \int_{y_k^{(j)}}^{\xi} + \int_{\xi}^{y_{k+1}^{(j)}} + \dots + \int_{y_{m_j}^{(j)}}^{+\infty}$$
(B.3)

(in strip 2 there is no need to consider intervals with ξ). The integration variable can be changed to be $t=\hat{t}_j$, with $dt=\hat{t}_j'dx$ and in this new variable it is apparent that all the contributions corresponding to the intervals (B.3) vanish because $\hat{t}_j(y_k^{(j)})=0$, except the first and the last. This leads to

$$S_{j} = \int_{\hat{t}_{j}(-\infty)}^{\hat{t}_{j}(+\infty)} dt \left(\frac{\log|1+t|}{t} - \frac{\log|t|}{1+t} \right).$$
 (B.4)

Along the flow $(\xi \in \mathbb{R})$, the required endpoints of the integral take the following values:

$$\hat{t}_j(+\infty) = 2\cos\lambda = \frac{1+\sqrt{5}}{2},$$

$$\hat{t}_1(-\infty) = s_1 \log \hat{g}_1(-\infty, \xi) = -1, \qquad \hat{t}_2(-\infty) = 0.$$
(B.5)

The integral itself is recognised to be a sum of Rogers dilogaritms that, at the previous endpoints, can be exactly computed. Actually only the sum is required:

$$S_1 + S_2 = \frac{11}{15}\pi^2. (B.6)$$

On the other hand, one can substitute in (B.2) the expressions for ϵ_j , ϵ'_j given by the TBA equations (4.3, 4.4). In doing this, all terms involving the convolution have cancelled because of the symmetry of the kernel, K(x) = K(-x). Among the remaining terms, those involving the derivatives L'_j are integrated by parts leading to

$$S_1 + S_2 = -2 \int_{-\infty}^{+\infty} dx \left[\sum_{k=1}^{m_1} \frac{L_1}{\sinh(y_k^{(1)} - x)} + \sum_{k=1}^{m_2} \frac{L_2}{\sinh(y_k^{(2)} - x)} - 4e^{-x} L_2 \right] + 2 \int_{-\infty}^{+\infty} dx \frac{\hat{g}_1'}{\hat{g}_1} L_1.$$
 (B.7)

The first term on the right hand side enters the expression for the energy (B.1). Using the result (B.6) one obtain, for all $\xi \in \mathbb{R}$:

$$E(\xi) = -\frac{11}{120} + \frac{\mathbf{m}^T C \mathbf{m}}{4} + \sum_{i=1}^2 \sum_{k=1}^{m_j} I_k^{(j)} - \frac{i}{2\pi} \sum_{k=1}^{m_2} \log \hat{g}_1(y_k^{(2)} - i\frac{\pi}{2}, \xi) + \int_{-\infty}^{+\infty} \frac{dx}{4\pi^2} \frac{\hat{g}_1'}{\hat{g}_1} L_1.$$
 (B.8)

This is the espression for the energy with the most explicit dependence on the boundary term \hat{g}_1 so that is well suited to the purpose of taking the limit $\xi \to +\infty$. Using the explicit expression for \hat{g}_1 and remembering that, along the flow, $y_1^{(2)} = -\infty$ if and only if $I_1^{(2)} = n_2$, one obtains

$$\lim_{\xi \to +\infty} -\frac{i}{2\pi} \sum_{k=1}^{m_2} \log \hat{g}_1(y_k^{(2)} - i\frac{\pi}{2}, \xi) = \lim_{\xi \to +\infty} -\frac{i}{2\pi} \sum_{k=1}^{m_2} \log \tanh(\frac{y_k^{(2)} + \xi}{2} - i\frac{\pi}{4}) = -\frac{1}{2} \delta_{I_1^{(2)}, n_2}. \quad (B.9)$$

This term is the new feature of the flow under examination with respect to the cases with single character. In spite of the fact that $\lim_{\xi \to +\infty} \hat{g}'_1 = 0$, the term under the integral also gives a contribution because of the divergence $L_1(-\infty) = \log 0 = -\infty$ (B.5). From the TBA equations the following asymptotic behaviour is obtained, for all fixed values of ξ

$$\epsilon_1(x) \underset{x \sim -\infty}{\sim} - \log \tanh \frac{x + \xi}{2}.$$
(B.10)

To get this from (4.3), one considers that $y_k^{(1)} \gg -\infty$ because of the infinite number of 2-strings appearing in the scaling limit [1]. In addition to that, $L_2(-\infty) = 0$ was used. Actually, the following term will be used:

$$L_1' = -\frac{s_1 e^{-\epsilon_1} \epsilon_1'}{1 + s_1 e^{-\epsilon_1}} \underset{x \sim -\infty}{\sim} \frac{1}{2} (1 + \tanh \frac{x + \xi}{2}).$$
 (B.11)

This asymptotic behaviour in the variable x is relevant in the integral term in (B.8), when $\xi \to +\infty$. This is apparent from the following explicit expression:

$$\mathcal{I} \equiv \int_{-\infty}^{+\infty} \frac{dx}{4\pi^2} \frac{\hat{g}_1'}{\hat{g}_1} L_1 = -\int_{-\infty}^{+\infty} \frac{dx}{4\pi^2} \log|\hat{g}_1| L_1' = -\int_{-\infty}^{+\infty} \frac{dx}{4\pi^2} \log|\tanh\frac{x+\xi}{2}| L_1'$$
 (B.12)

where an integration by parts has been performed and the corresponding boundary terms vanish. One has:

$$\mathcal{I} \underset{\xi \sim +\infty}{\sim} -\frac{1}{2} \int_{-\infty}^{+\infty} \frac{dx}{4\pi^2} \log|\tanh \frac{x+\xi}{2}| (1+\tanh \frac{x+\xi}{2})$$

$$= -\int_{-\infty}^{+\infty} \frac{dx}{4\pi^2} \log|\tanh x| (1+\tanh x)$$

$$= -\int_{-\infty}^{+\infty} \frac{dx}{4\pi^2} \log|\tanh x| = -\int_{0}^{+\infty} \frac{dx}{2\pi^2} \log \tanh x \qquad (B.13)$$

where on the first line the asymptotic behaviour was used, in the second line a redefinition of x shows that the integral is independent on ξ , on the third line a term vanish because it is odd under the exchange $x \to -x$; the remaining integrand is even under the same exchange and this leads to the last equality. With a new change of variables, this definite integral is transformed in

$$\mathcal{I} = -\int_0^1 \frac{dt}{4\pi^2} \frac{1}{t} \log \frac{1-t}{1+t} = \frac{1}{16}.$$
 (B.14)

The actual value can be explicitly computed or obtained from standard mathematical tables of integrals; it admits also an expression in terms of Rogers dilogarithms. In conclusion, from (B.8, B.9, B.14) one has the energy at the IR critical point $(1,1) \oplus (3,1)$

$$E = -\frac{7}{240} + \frac{\mathbf{m}^T C \mathbf{m}}{4} - \frac{1}{2} \delta_{I_1^{(2)}, n_2} + \sum_{i=1}^2 \sum_{k=1}^{m_i} I_k^{(i)}$$
(B.15)

that is precisely the expression (2.7) given in Section 2. The first term is the central charge contribution $-\frac{c}{24}$.

As a final comment, the expression (B.8) can be generalized to all the flows with the obvious addition of terms depending upon \hat{g}_2 and a possibly non-zero term that takes into account the subtleties related to $\hat{t}_1(-\infty)$.

Appendix C. Rule for the integration constants s_i .

The braid limit used in the first line of (B.5) can be used to obtain the general selection rule for the variables s_j . They appear in the derivation of the TBA equations as integration constants (see [1] for details). Then, taking the limit $x \to +\infty$ in the equations themselves, one can use the braid limit to express the asymptotic values of ϵ_j , L_j . This leads to:

$$s_j = (-1)^{m_j}, \qquad \xi \in \mathbb{R}, \ \xi = +\infty = \text{IR}.$$
 (C.1)

An implicit assumption was used, that all the 1-strings are in a finite position, $y_k^{(j)} < +\infty$, condition that is always satisfied except at the UV point. If this is violated, the actual value of the braid limit can change and the previous argument doesn't hold. The correct UV rule can be obtained by the previous one observing that if along the flow one has $\hat{g}_j \neq 1$, the content of zeros changes in the strip 3-j so that:

$$s_j = (-1)^{m_j + 1}, \qquad \xi = -\infty = \text{UV}.$$
 (C.2)

The selection rules proven here hold for all the flows and all the conformal boundary conditions. Of course, they contain the cases given in [1] and, in this sense, this Appendix completes the exposition given there.

References

- [1] G. Feverati, P.A. Pearce and F. Ravanini, Nucl. Phys. B675 (2003) 469.
- [2] S. Ghoshal and A. B. Zamolodchikov, Int. J. Mod. Phys. A9 (1994) 3841.
- [3] J.L. Cardy, Nucl. Phys. **B324** (1989) 481.
- [4] K. Graham, I. Runkel and G.M.T. Watts, hep-th/0010082; P. Dorey, M. Pillin, A. Pocklington, I. Runkel, R. Tateo, G.M.T. Watts, hep-th/0010278. Talks given at *Nonperturbative Quantum Effects 2000*.
- [5] L. Chim, Int. J. Mod. Phys. **A11** (1996) 4491.
- [6] I. Affleck, J. Phys. **A33** (2000) 6473.
- [7] A. Recknagel, D. Roggenkamp, V. Schomerus, Nucl. Phys. **B588** (2000) 552.
- [8] S. Fredenhagen and V. Schomerus, Phys. Rev. D67 (2003) 8500; S. Fredenhagen, Nucl. Phys. B660 (2003) 436.
- [9] R.I. Nepomechie, Int. J. Mod. Phys. A17 (2002) 3809.
- [10] R.I. Nepomechie and C. Ahn, Nucl. Phys. **B647** (2002) 433.
- [11] E. Melzer, Int. J. Mod. Phys. A9 (1994) 1115; A. Berkovich, Nucl. Phys. B431 (1994) 315.
- [12] D.L. O'Brien, P.A. Pearce and S.O. Warnaar, Nucl. Phys. **B501** 773 (1997).
- [13] R.E. Behrend and P.A. Pearce, J. Stat. Phys. **102** (2001) 577.
- [14] R.E. Behrend, P.A. Pearce, V.B. Petkova and J.B. Zuber, Nucl. Phys, **B579** (2000) 707.
- [15] P.A. Pearce, L. Chim and C. Ahn, Nucl. Phys. B601 (2001) 539; Nucl. Phys. B660 (2003) 579.